Title

Geometry matters for sonic tomography of trees

Authors

Daniel C. Burcham[1]*, Nicholas J. Brazee[2], Robert E. Marra[3], Brian Kane[4]

[1]Centre for Urban Greenery and Ecology

National Parks Board

Singapore 259569

[2]Center for Agriculture, Food, and the Environment

University of Massachusetts Amherst

Amherst, MA 01003

[3]Department of Plant Pathology and Ecology

Connecticut Agricultural Experiment Station

New Haven, CT 06504

[4]Department of Environmental Conservation

University of Massachusetts Amherst

Amherst, MA 01003

*Corresponding author: daniel.burcham@colostate.edu

Department of Horticulture and Landscape Architecture

Colorado State University

Fort Collins, CO 80523

Abstract

For trees growing in communities, arborists routinely check for evidence of damaged wood during tree risk assessment, and sonic tomography is occasionally used to measure the amount of internal damage in trees. Existing studies investigating the accuracy of commercially available sonic tomography devices have mostly considered a limited range of measurement conditions, limiting their application in practice. Using measurements incorporating greater variability in test conditions, this study examined the accuracy of sonic tomography by comparing the percent damaged cross-sectional area in tomograms with the destructively measured internal condition of trees. Although the accuracy of tomograms differed between the examined temperate and tropical tree species, the variation was largely explained by underlying differences in the cross-sectional geometry of the measured tree parts. The amount of decay was repeatedly underestimated in measurements of small, circular cross sections, and, conversely, it was consistently overestimated in measurements of large, irregularly shaped cross sections. Using different approaches to generating and interpreting tomograms, a wide range of decay estimates was obtained for a given set of measurements. By adjusting software settings, it was possible to obtain tomograms with the least error for a given cross-sectional geometry, and the tomograms could be visually interpreted to similarly compensate for the anticipated measurement error. Although practitioners can use the identified strategies to compensate for the expected measurement error in different situations, there is also a fundamental need to develop improved measurement and analysis routines for sonic tomography relying on physically realistic assumptions about acoustic wave propagation in wood.

Keywords

Cross-sectional geometry; Decay; Image analysis; Risk assessment; Tomogram; Wave velocity

Key Message

Due to the simplifying assumptions used to analyze acoustic wave propagation in trees, the accuracy of sonic tomograms varies significantly according to the geometry of the measured tree part.

Acknowledgments

The authors gratefully acknowledge Ms. Clarice Xu Huiyue and Mr. Robin Ong for their practical assistance with sonic tomography and destructive verification in Singapore.

Introduction

When present, internal decay, cracks, and cavities may decrease the load-bearing capacity of tree parts, and damaged wood is often an important concern during tree risk assessment (Smiley et al. 2017). After discovering evidence of internal defects, practitioners occasionally use sonic tomography to measure the amount of internal damage in standing trees (Johnstone et al. 2010). By measuring the apparent speed of acoustic stress waves transmitted through a tree part, sonic tomography estimates the extent of damaged wood associated with relatively low acoustic transmission speeds (Arciniegas et al. 2014).

The information contained in sonic tomograms must be reliable to inform tree management decisions, especially if internal damage is a governing consideration for tree risk assessment. During tree risk assessment, the amount of information available to arborists can influence their judgments about the risk presented by a tree, but the availability of additional information, without clear guidance on the interpretation of data, may not always lead to agreement among arborists assessing tree risk (Koeser et al. 2017). Despite numerous validation studies of sonic tomography (Wang et al. 2009; Brazee et al. 2011; Liang and Fu 2012a; Ostrovsky et al. 2017), the contributions of various factors towards measurement uncertainty remain poorly understood.

Recent work showed that sonic tomography can be used to estimate the decreased load-bearing capacity of damaged tree parts, but the limitations of the technique must be considered when it is used for this purpose (Burcham et al. 2019). Several existing studies, mostly involving measurements of cylindrical tree parts in temperate climates, compared sonic tomograms with the destructively measured internal condition of trees (Wang et al. 2009; Brazee et al. 2011; Li et al. 2012; Ostrovsky et al. 2017). Although tomograms generally depicted internal features correctly, some authors reported that sonic tomography underestimated the size of decayed areas (Liang et al. 2007; Wang et al. 2009; Burcham et al. 2019) and overestimated the size of cracks (Wang et al. 2007b), but the measurement of cracks also depends on the type of discontinuity, such as radial or ring shakes, and the position of acoustic sensors. These studies usefully assisted the interpretation of tomograms by documenting the performance of various commercial devices, but most studies were limited to small sample sizes incorporating modest variability across the range of all possible measurement conditions (Gilbert and Smiley 2004; Wang et al. 2007b, 2009; Li et al. 2012; Liang and Fu 2012b).

Some studies have reported challenges using sonic tomography on large stems with irregular cross-sectional geometries (Rabe et al. 2004), including buttressed tropical trees (Gilbert et al. 2016). For such trees, it is increasingly difficult to determine the location of measurement positions around the tree, especially using some methods provided by manufacturers of commercial devices (Rust 2017). Under these circumstances, the simplifying assumption that acoustic stress waves propagate along straight paths is more commonly violated (Gilbert et al. 2016), and the prediction error between the apparent and actual acoustic speeds worsens. These challenges are practically significant because arborists often measure the extent of decay near the root flare, where severe decay (Schwarze et al. 2000) and large wind-induced bending moments (Ennos 2012) commonly occur. Given the importance of decay assessment with sonic tomography for tree risk management, this study examined the accuracy of sonic tomography across a wide range of measurement conditions, including tree parts with varied cross-sectional geometries, to guide the interpretation of sonic tomograms during decay assessment. Given the device's simplifying assumptions about acoustic wave propagation in wood, it was expected that measurement error would be greater for large, irregularly shaped trees. In addition, the possible use of techniques for managing measurement uncertainty was evaluated by systematically examining changes in the accuracy of tomograms using different software settings and interpretation strategies.

Methods

Sites and trees

Trees showing obvious indicators (e.g., fruiting structures, cavities) of internal decay were selected for use in this study from two different sites, including a temperate deciduous forest in northwest

Connecticut, USA and tropical urban landscapes in Singapore. The distinct size distribution and species composition of trees growing on the two sites allowed a combined sample of tomograms with considerable variability in measurement conditions, especially the cross-sectional geometry of tree parts. In total, 41 individual trees from three temperate (*Acer saccharum*, *Betula alleghaniensis*, *Fagus grandifolia*) and seven tropical (*Khaya grandifoliola*, *Lonchocarpus sericeus*, *Peltophorum pterocarpum*, *Pterocarpus indicus*, *Sandoricum koetjape*, *Syzygium grande*, *Tamarindus indicus*) species were examined using sonic tomography. The temperate trees were selected during a site survey to identify trees for a separate experiment in 2014, and the tropical trees were identified opportunistically from scheduled tree removals between 2018 and 2020. All trees had a diameter at breast height (1.37 m above ground) exceeding 0.3 m. See Marra et al. (2018) for more information about the trees selected from Connecticut.

Sonic tomography and destructive measurements

Using a PiCUS® Sonic Tomograph 3 (IML Electronic GmbH, Rostock, Germany), sonic tomography was used to estimate the internal condition of each tree at one or more locations distributed along the lower trunk (see supplementary materials for the species, measurement height, and geometry of individual cross sections). The measurements were conducted by following the manufacturer's instructions, and the location of each sensor position was determined using the free shapes geometry workflow in the PiCUS® Q74 software with distance measurements obtained from the PiCUS® caliper. The acoustic sensors were distributed around the perimeter of each cross section at an average density of 5.4 sensors$\cdot$m^{-1}, within the range (2.5 – 6.7 sensors$\cdot$m^{-1}) recommended by the manufacturer. For each set of measurements, tomograms were generated using the two calculation settings (SoT 1 and SoT 2) available in the software, and the color scale for each resulting tomogram was displayed using either the default (50%) or expanded (0%) maximal color space. Using the expanded maximal color space, the tomogram color scale was distributed over the entire range of apparent acoustic speeds, instead of only illustrating limited variation in apparent acoustic speeds up to 50% of the reference speed. SoT 1 is the default tomogram calculation setting in the Q74 software. Using the assumed linear travel paths between sensors, the software determines the apparent speed at each path intersection as the fastest value among all measurements passing through the same point. The SoT 1 calculation setting uses the resulting set of apparent speeds for image reconstruction, but the SoT 2 calculation additionally detects and removes artefacts caused by erroneous slow intersections before image reconstruction. In some cases, the additional step in the analysis process reduces the size of areas with relatively slow apparent speeds in tomograms created using SoT 2. Apart from general details, the manufacturer does not provide detailed information allowing an independent implementation of the entire analysis process. In total, four different tomograms were generated from each set of measurements using unique combinations of the software settings (SoT 1 – default, SoT 1 – expanded, SoT 2 – default, SoT 2 expanded). See the supplementary materials for examples of tomograms created using the four software settings.

After tomographic measurement, the trees were felled and sectioned at the location of each tomogram, and each exposed cross section was photographed, using an XE3 camera (Fujifilm Corporation, Tokyo, Japan) with a 14 mm lens, with a scale reference and the camera lens orthogonal to the cross section. Subsequently, the digital images were manually binarized, by selecting specific objects using the quick selection tool in Photoshop (Adobe, San Jose, CA), into black (0) and white (1) images depicting the absence or presence, respectively, of solid, undamaged wood (Figure 1). During binarization, the visible features associated with fungal decomposition (e.g., discoloration, pigmentation, zone lines, cavities) were used to manually identify damaged wood, and the region enclosed by the outer trunk boundary, excluding the bark, was used to define the maximum possible extent of solid wood. The use of visible features to determine the extent of internal damage is consistent with most existing studies (Gilbert and Smiley 2004; Brazee et al. 2011; Liang and Fu 2012b; Ostrovsky et al. 2017). For some tropical trees, longitudinal internal voids were formed by natural grafting between adjacent buttress roots during secondary growth (Figure 1), and these features, distinguished by the presence of bark on the enclosed interior surfaces, were classified as damaged wood during binarization, since they would similarly impede acoustic wave transmission.

The accuracy of sonic tomography was examined by comparing each sonic tomogram with its paired binary image of the measured cross section. Although the interpretation of sonic tomograms may require the examination of several different diagnostic features, the amount of decay was primarily used to examine agreement between sonic tomograms and binary images in this study, since it largely explained errors in strength loss estimates derived from tomograms in an earlier analysis of measurements from the temperate species (Burcham et al. 2019). For each tomogram and binary image, the percent total damaged cross-sectional area, A_D (%), was computed, using the image processing and numerical analysis procedure outlined by Burcham et al. (2019). Briefly, the solid and damaged regions in each tomogram were selected using specific color ranges in the HSV or LAB color space associated with the blue trunk boundary outline or visualized decay pattern, and a binary mask was created by assigning positive binary values (1) to all pixels containing values within the specified ranges. After the binarization tomograms and photographs (described earlier), the boundaries of features in binary images were traced to produce a list of coordinates for the perimeter of each shape, and the intrinsic image coordinates (row, column) were converted to Cartesian coordinates (x, y) using a reference object relating the physical extent of each pixel. The resulting set of n clockwise-ordered coordinate pairs described a simple, closed curve enclosing a region of solid or damaged wood.

Two different color combinations were used to select damaged parts in sonic tomograms: green, violet, and blue (GVB) and violet and blue (VB). In PiCUS® sonic tomograms, green demarcates transitional areas between damaged and solid wood with intermediate apparent speeds, and the damaged area reported by the software consistently excludes green from estimates. However, the binary treatment required a classification for all areas in tomograms, and the two extreme cases – including and excluding all green areas – were examined in this study. For each estimate, A_D(error) was computed as the difference between A_D determined from sonic tomograms and A_D determined from the corresponding binary image. Using this formulation, a positive and negative A_D(error) indicated an overestimate and underestimate, respectively, of the actual amount of decay using sonic tomography.

To examine the effect of the cross-sectional geometry of measured tree parts on A_D(error), several geometric properties were estimated using the trunk boundary outline obtained from the binary image of each tree. For each binary image, the cross-sectional area, A (m^2), was computed using:

$$A = 1/2 \sum_{i=1}^{n} (x_i y_{i+1} - x_{i+1} y_i), \quad \text{Eq. 1}$$

where (x_i, y_i), $\{i \mid \in 1 \ldots n\}$, are the coordinate pairs of the solid trunk boundary outline. See Burcham et al. (2019) for a detailed summary of the image analysis procedure for extracting boundary coordinates. In addition, three dimensionless measures of shape, unaffected by scale and orientation, were used in this study. The resemblance of each cross-sectional shape to an idealized circle was assessed using circularity, C:

$$C = 4\pi A / P^2, \quad \text{Eq. 2}$$

where P (m) is the perimeter of the shape:

$$P = \sum_{i=1}^{n} \sqrt{(x_{i+1} - x_i)^2 + (y_{i+1} - y_1)^2}. \quad \text{Eq. 3}$$

The convexity of each cross-sectional shape was assessed by computing its solidity, S:

$$S = A / A_{conv}, \quad \text{Eq. 4}$$

where A_{conv} is the cross-sectional area of the convex hull (Barber et al. 1996) for the same shape. Using this definition, S will be relatively low and high for concave and convex shapes, respectively. The eccentricity, E, of each cross-sectional shape was examined using:

$$E = \sqrt{1 - (\min(\mathbf{V}) / \max(\mathbf{V}))^2}, \quad \text{Eq. 5}$$

where $\mathbf{V}$ is a column vector containing the eigenvalues of the covariance matrix computed from the list of boundary coordinates for each cross section. In this formulation, the principal axes of the shape coordinates were used to construct an ellipse, and E was defined as the aspect ratio of the distance between the ellipse foci and major axis length. For each case, the eigenvalues were inspected to ensure none of the values were repeated. All image processing and numerical analyses were performed in MATLAB R2019b (MathWorks, Natick, MA, USA).

Statistical analysis

Two linear models were fit to the data. First, analysis of variance (ANOVA) was used to examine differences in A_D(error) among sonic tomography measurements conducted on the four species with the greatest number of observations, after excluding data from species with fewer than three observations. The analysis was conducted using measurements obtained from tomograms generated using the default settings (SoT 1 – default) of the PiCUS® Q74 software, and only violet and blue (VB) were used to select damaged parts in tomograms, consistent with the default settings in the software. The model had one fixed effect with four levels (species: *A. saccharum*, *B. alleghaniensis*, *F. grandifolia*, *P. indicus*), and mean separation was performed, as necessary, using Tukey's Honestly Significant Difference test.

Second, analysis of covariance (ANCOVA) was used to examine the effect of software settings (SoT 1 – default, SoT 1 – expanded, SoT 2 – default, SoT 2 – expanded) and tomogram color interpretation (GVB, VB) on A_D(error), after accounting for the cross-sectional geometry of measured tree parts. For a given geometry, the analysis sought to determine the software settings, which are used to generate tomograms, and color combinations, which are used to distinguish damaged from undamaged wood, that produced the most accurate diagnostic assessment of a tree's internal condition. Other than adjustments to the calculation settings and color space, all other software settings were maintained at their default values. The geometric properties were highly correlated with one another, with Pearson correlation coefficients exceeding 0.5 in all pairwise cases, and principal component analysis (PCA) was used to avoid fitting models affected by multicollinearity by reducing the dimension of a set of highly correlated covariates. The linear combination of geometric properties summarizing a majority of variance in their values was subsequently used as a covariate in model development. To ensure data from each treatment were adequately described by a linear regression model, the normality and homogeneity of errors were examined by inspecting plots of residuals against the dependent variables, and the suitability of a linear function was assessed using the *F*-test for lack of fit (Kutner et al. 2004). The covariates exhibiting a significant linear relationship with A_D(error) were retained in the model. For the selected covariate(s), the homogeneity of slopes among levels of the fixed effect was tested and, if rejected, an unequal slopes model was used for the associated covariate. Fixed effects were tested at the mean value of the selected covariates. For significant fixed effects, LS means were computed using multiple values over the observed range of each selected covariate, and mean separation was performed using Tukey's Honestly Significant Difference test at specific combinations of the covariate values. Statistical analyses were performed using SAS 9.4 (SAS Institute, Inc., Cary, NC, USA) using proc mixed.

Results

Geometry of measured cross sections

The average cross-sectional area of tree parts examined in this study was much greater for tropical than temperate species (Table 1). In addition, the cross-sectional shape of tree parts measured on tropical species was, on average, much less circular and more concave, with more portions of the trunk perimeter curved inward between buttress roots or other features. Although the tropical cross sections were, on average, more eccentric than their temperate counterparts, the eccentricity of temperate and tropical cross sections extended over a similar range of values. After felling, visual inspection showed decay, discoloration, and cavities occasionally present in the measured cross sections, but none of the cross sections contained large cracks. On average, the decay columns occupied a similar proportion of the cross-sectional area among temperate and tropical species.

Accuracy of sonic tomograms

Among all sonic tomography measurements, A_D(error) varied between -52.8% and 87.7%, with the actual amount of damaged wood occasionally minimized or exaggerated in tomograms, depending on the software settings and tomogram color interpretation. Using the default software settings (SoT 1 – default) to generate tomograms, ANOVA showed that mean A_D(error) varied significantly among species (Table 2), assuming only violet and blue (VB) depicted damaged areas. Compared to the binary images, A_D(error) was consistently negative and positive in tomograms generated from measurements of the temperate and tropical species, respectively. Although there was not a significant difference in mean A_D(error) among the three temperate species, the average A_D(error) for the tropical *P. indicus* was significantly greater than all three temperate species.

Influence of cross-sectional geometry on tomogram accuracy

Alongside differences in A_D(error) between the temperate and tropical species, the accuracy of tomograms covaried with all of the analyzed measurements of cross-sectional geometry. For all settings and colors used to process and interpret tomograms, there were significant correlations between A_D(error) and A, C, S, and E (Figure 2). A_D(error) was positively correlated with A and E and negatively correlated with C and S. For all treatment combinations, linear regression showed a significant linear relationship between A_D(error) and each size or shape variable. Among the three shape variables, the average rate of change in A_D(error) was greatest over a unit change in S, and C and S consistently accounted for greater variability in A_D(error) than other geometric variables (Table 3). In contrast, the regression models showed weaker relationships between A_D(error) and other variables; E consistently explained the least amount of variability in A_D(error). For all regression models, the residuals appeared normally and uniformly distributed, and there was no evidence of a lack of fit using a linear function to model relationships.

After testing all covariates in a factorial model, A ($F = 2.66$; df = 8, 536; $p = 0.007$), C ($F = 4.85$; df = 8, 536; $p < 0.001$), and S ($F = 3.28$; df = 8, 536; $p = 0.001$) were selected to account for the relationship between A_D(error) and cross-sectional geometry, but they were all highly correlated with one another ($|r| > 0.75$). Using PCA, A, C, and S were linearly combined along a single axis accounting for 90% of variance in the three-variable space; the derived factor, depicting geometric variation in size and shape variables, was negatively loaded with *A* (-0.91) and positively loaded with *C* (0.97) and *S* (0.95), with positive and negative values along the derived axis representing small, circular, convex and large, non-circular, concave shapes, respectively. The slopes describing the change in A_D(error) over a unit change in the geometry covariate, *G* (dimensionless), obtained using PCA varied significantly between the examined software settings ($F = 32.36$; df = 3, 563; $p < 0.001$) and tomogram colors ($F = 18.49$; df = 1, 563; $p < 0.001$), and unequal slopes were used to describe the relationship between A_D(error) and *G* for each software setting and tomogram color set. For estimates obtained using each of the calculation settings and tomogram colors, the slope coefficients showed A_D(error) decreased over a unit change in *G*, but rate of change in A_D(error) was greatest for the default software settings (SoT 1 – Default) and larger color set (GVB) (Table 4).

After accounting for the cross-sectional geometry of the measured tree parts, ANCOVA showed that the accuracy of tomograms, in terms of A_D(error), was, at the mean value of the geometry covariate ($G = 0$), significantly affected by the various software settings and colors used to generate and interpret tomograms, but the different measurement configurations did not interact with one another to affect A_D(error) (Table 4). Mean separation was performed at three values spanning the range of *G* observed in the data. At three values of the covariate, the mean A_D(error) associated with the four software settings used to produce tomograms varied inconsistently (Table 5). At $G = -2.77$, there were significant differences among mean A_D(error) associated with the four software settings used to produce tomograms, except for tomograms displayed using the expanded and default maximal color space for the SoT 1 and SoT 2 calculation settings, respectively. At $G = 0$, the mean A_D(error) varied significantly between all software settings used to produce tomograms. At $G = 0.85$, there was a significant difference in mean A_D(error) between tomograms displayed using the expanded and default maximal color space for the SoT 1 and SoT 2 calculation settings, respectively, but the mean A_D(error) did not significantly vary among the remaining software settings. Unsurprisingly, the mean A_D(error) was also significantly different between the two color combinations used to select damaged parts in tomograms, since the measurements used different portions of the images.

Strategies for managing measurement uncertainty

The formulation of A_D(error) indicated that the accuracy of tomograms increased as values approached zero, and the LS means showed that the most suitable choice of measurement configurations for sonic tomography depended on the cross-sectional geometry of the measured tree part (Table 5). For all cross-sectional areas, A_D(error) was consistently positive (damage overestimated) and negative (damage underestimated) on large, non-circular, concave (G = -2.77) and small, circular, convex (G = 0.85) cross-sectional shapes, respectively. A_D(error) moderated towards zero as G decreased below zero, and the A_D(error) associated with some software settings was not significantly different from zero in some cases. For $G > 0$, A_D(error) was minimized by using the SoT 1 calculation settings with the default maximal color space (SoT 1 – default) and a larger portion of the tomogram color set (GVB) to compensate for the underestimated damaged area. In contrast, A_D(error) progressively worsened towards greater positive values as the size of non-circular, concave cross sections increased. For $G << 0$, A_D(error) was minimized by using the SoT 2 calculation settings with the expanded maximal color space (SoT 2 – expanded) and a smaller portion of the tomogram color set (VB) to compensate for the overestimated damaged area.

Discussion

This study demonstrated considerable differences in the accuracy of sonic tomography over a range of measurement conditions for one commercially available device. Consistent with most existing studies, the decayed area in small cylindrical cross sections was repeatedly underestimated in sonic tomograms (Gilbert and Smiley 2004; Deflorio et al. 2008; Wang et al. 2009; Liang and Fu 2012b; Marra et al. 2018; Burcham et al. 2019), but the accuracy of sonic tomography was very different for measurements of large, irregularly-shaped cross sections, with the amount of decay repeatedly overestimated, by as much as 87.7%, in sonic tomograms. Although other studies reported that cracks were overestimated in sonic tomograms (Wang et al. 2007b), the possibility of tomograms inaccurately depicting an excessive amount of decay has not been previously reported. In this study, the visual binarization process may have inaccurately classified some parts of the examined cross sections, especially the advancing margins of the decay column containing early stages of fungal decomposition. However, the presence of advanced decomposition was visually obvious throughout most of the decay columns examined in this study, and it is unlikely that the observed patterns in the accuracy of tomograms were strongly altered by classification error during binarization. In the future, it will also be useful to compare visual classification with quantitative measurements, such as hardness (Liang and Fu 2012b) or density (Rabe et al. 2004), for determining the accuracy of sonic tomograms.

Although the accuracy of sonic tomograms varied between the tropical and temperate tree species examined in this study, the divergent error rates were largely explained by underlying differences in the cross-sectional geometry of measured tree parts. Compared to temperate forests, the greater prevalence of buttressing among trees growing in lowland tropical forests has been extensively documented (Davis and Richards 1934; Smith 1972), and it will be important for arborists, especially in the lowland tropics, to appreciate the contrasting expectations for the accuracy of sonic tomography in different situations. It will be valuable to confirm the results in this study with additional observations from tree parts with a range of cross-sectional geometries, but the discrepancy between temperate and tropical measurements illustrates the importance of studying similar issues outside conditions adequately represented in existing studies, especially temperate North America and Europe. In one existing study, Ostrovsky et al. (2017) reported that the accuracy of sonic tomograms was not affected by the eccentricity or size of the measured cross sections, but the study used observations mostly confined to small trees with regular cross-sectional shapes.

There are several possible explanations for the observed differences in error rates. On large, irregularly shaped cross sections, it may be increasingly difficult to accurately measure the two variables required to compute apparent speed (i.e., travel distance and time). The location of acoustic sensors around the tree perimeter must be determined accurately because most devices infer travel distance from the pairwise linear distances between all sensors. Among existing commercial devices, the caliper triangulation process for geometry measurement is less susceptible to error on non-circular trees (Rust 2017), and there are several promising alternative geometric measurement techniques worth considering (Rust 2021). In addition to improving the accuracy of such measurements, there is a need to increase the speed and productivity of geometry measurement workflows for sonic tomography, since it is one of the most time-consuming tasks in a lengthy process (Balas et al. 2020). The PiCUS® software manual recommends installing sensors uniformly around the perimeter of the cross section with a spacing between 15 and 40 cm, and the sensors should be situated on the outermost extent of individual buttresses and the innermost part of adjacent indentations. Especially for the irregularly shaped trees, it was occasionally necessary to adjust the placement of sensors to allow for their installation or measurement with the calipers, and the lack of conformity with recommendations may have contributed to unknown error in some tomograms.

In addition, the measurement and image reconstruction techniques used by some commercial devices to produce tomograms rely on the assumption that acoustic waves propagate along straight rays through an isotropic medium (Arciniegas et al. 2014), but wood transmits acoustic waves at different speeds in the three principal directions along which it is organized (Schubert et al. 2009), resulting in curved pathways (Espinosa et al. 2019, 2020b). Although several researchers have proposed new inversion algorithms accounting for material anisotropy (Maurer et al. 2006; Liu and Li 2018; Espinosa et al. 2020a), the methods are not commercially available for practical use, and there is a need for more work to examine the reliability of new techniques and identify opportunities for further improvement. In decayed trees, altered wood material properties caused by the host-fungus interaction also distort acoustic wave propagation. Decomposed wood is often surrounded by reaction zones containing antimicrobial polyphenolic deposits and, occasionally, barrier zones containing highly suberized tissue (Pearce 1996), and the associated heterogeneity in material properties further confounds methods used for image reconstruction. For the PiCUS®, the manufacturer provides limited information about the differences between the calculation settings used to produce tomograms, but they recommend using SoT 2 in most situations, except for trees with incipient or brittle decayed wood, often caused by *Kretzschmaria deusta* infections (Schwarze et al. 1995), situated near the center of the tree part.

Apart from material anisotropy and heterogeneity, the assumption of straight travel paths is additionally violated on concave cross sections, since the acoustic waves must travel around indentations between adjacent buttress roots (Gilbert et al. 2016), and this likely explains the strong relationship between A_D(error) and S observed in this study. The lowest solidity values were generally observed on trees with large buttress roots, and the manufacturer recommends installing sensors on all three sides of a buttress root to estimate apparent speeds for the associated areas. However, the protruding buttresses often complicate measurements of nearby sensors with the calipers, and the additional sensors may not compensate for the incorrect path trajectories near buttresses.

In future work, it will be important to examine the influence of other factors on the accuracy of sonic tomography, such as the size and position of decay columns with respect to acoustic sensors. For example, an acoustic wave's short deviation around small decayed areas creates a small increase in travel time and, given the assumed straight travel paths, a modest decrease in apparent speed, but the sensitivity of the image reconstruction process to small differences in apparent speed could affect the accuracy of the resulting tomogram. Some authors reported that tomogram accuracy generally improved with the number of uniformly-distributed acoustic sensors (Divos and Divos 2005; Liang and Fu 2014), but the marginal improvement in tomogram accuracy diminished noticeably with more than 12 sensors on small, round tree parts with diameters between 20 and 30 cm (Divos and Divos 2005). Since measurement effort increases with additional sensors, it will be important to develop strategies for installing limited acoustic sensors to create a relatively uniform distribution of path intersections, especially for large, irregularly shaped tree parts.

Even without a clear explanation for the different error rates, it is important to document and report the limitations of sonic tomography to better inform tree risk management decisions. In many cases, the information contained in sonic tomograms is used to estimate the decreased load-bearing capacity of the measured tree part, and the practical implications of the observed measurement uncertainty for similar applications depends on the sign of A_D(error). For small, circular, convex cross sections, the negative A_D(error) will contribute towards an estimate of the load-bearing capacity exceeding the true value, and this may prevent the structural condition of the tree from receiving the attention it deserves. Conversely, the positive A_D(error) associated with large, non-circular, concave cross sections will contribute towards an inadequate assessment of the load-bearing capacity, and this may increase the possibility of intervening unnecessarily to mitigate the risk of tree failure, especially since larger tree parts can cause more severe consequences if they impact a target.

In the absence of additional work to improve devices, this study outlines several practical ways for arborists to minimize measurement error in their work. Depending on the cross-sectional geometry of the measured tree part, the software calculation settings can be adjusted to minimize A_D(error), and the tomograms can be interpreted using specific color ranges to further compensate for the anticipated measurement error. In this study, tomogram error was minimized for small, circular trees using the default software settings, but the alternate calculation settings (SoT 2) and expanded maximal color space improved tomograms, in terms of A_D(error), for large, irregularly shaped trees. The tomogram colors associated with the actual extent of decay also depended on the geometry of the measured tree part, and practitioners should consider the possible tendency towards under- and overestimating the extent of decay on small, circular and large, irregularly shaped cross sections, respectively, when interpreting tomograms. Since the measurements were generally more accurate on small, circular cross sections, arborists should account for the additional measurement uncertainty in their judgments when using sonic tomography on large, irregularly shaped cross sections. Beyond the basic software adjustments evaluated in this study, it may be possible to further refine tomograms by adjusting some of the other advanced software settings outlined in the PiCUS® user's manual, but many of the adjustments address specific data quality issues arising from the measurement or analysis of acoustic transmission speeds. It will be useful to examine the influence of other software manipulations on the accuracy of tomograms in future work.

Practitioners often use sonic tomography to measure the internal condition of the lower trunk near the expected location of severe decay, but it will also be important to consider the accuracy of sonic tomography when selecting a location for decay measurement. The tomograms may be more accurate at higher vertical positions on trees, since the trunk is often more circular and convex farther above ground, but the measurements will be most useful for tree risk assessment if they depict the weakest part of the tree. For concave cross sections, Gilbert et al. (2016) suggested that omitting buttress roots could avoid some of the measurement errors associated with sonic tomography on large, irregularly-shaped cross sections. By positioning acoustic sensors at the innermost part of the sinuses between buttress roots, the measured travel times would not be affected by acoustic waves propagating around indentations between buttress roots. However, it may not always be possible, depending on the shape of the cross section, to install sufficient sensors at the recommended density using this modified approach, possibly limiting the quality of tomograms (Wang et al. 2007a; Liang and Fu 2014). Moreover, the resulting diminutive tomogram, excluding buttress roots, could not be directly used to estimate the tree part's decreased load-bearing capacity – a common motivation.

Conclusions

Sonic tomography provides a reasonable, minimally invasive estimate of a tree's internal condition, but the accuracy of sonic tomography varied widely among observations in this study, depending on the cross-sectional geometry of the measured tree part. Given considerable differences in the accuracy of tomograms, practitioners should report the relevant test configurations and assumptions used to produce and interpret tomograms, alongside the anticipated measurement error for these choices, with their professional recommendations. To avoid judgments misled by measurement uncertainty, it will also be important to supplement sonic tomography measurements with additional, complementary evidence to make informed decisions about tree risk management. At the same time, there is a need to develop improved measurement and analysis methods, relying on robust assumptions about acoustic wave propagation in wood, for sonic tomography of trees. Despite longstanding challenges for measurement and modeling, the development of improved methods will diminish the problematic uncertainty currently confronted by practitioners using sonic tomography. It will also be important to conduct similar, comparative work on other commercially available devices, such as the Arbotom® (Rinntech-Metriwerk GmbH, Heidelberg, Germany) and ArborSonic 3D (Fakkop Enterprise Bt, Agfalva, Hungary), with measurements of damaged tree parts supplemented by test specimens constructed from synthetic materials.

Declarations

Funding

The National Science Foundation EArly-Concepts Grants for Exploratory Research (EAGER) Program (Grant #DEB-1346258) supported tomography and destructive measurements of temperate trees, and the National Parks Board, Singapore supported tomography and destructive measurements of tropical trees.

Author Contributions

Daniel Burcham conceptualized and designed the study. Daniel Burcham, Nicholas Brazee, and Robert Marra collected the data. Daniel Burcham analyzed the data and wrote the first draft of the manuscript, and all authors reviewed and edited the subsequent versions of the manuscript, including the final version.

Competing Interests

The authors have no relevant financial or non-financial interests to disclose.

Data and Code Availability

The data used in this study was deposited in the Harvard Dataverse (https://doi.org/10.7910/DVN/RGJFMR), and the MATLAB code used for image processing was uploaded to a public GitHub repository (https://github.com/danielburcham/geomProp).

Literature Cited

Arciniegas A, Prieto F, Brancheriau L, Lasaygues P (2014) Literature review of acoustic and ultrasonic tomography in standing trees. Trees Struct Funct 28:1559–1567

Balas M, Gallo J, Kunes I (2020) Work sampling and work process optimization in sonic and electrical resistance tree tomography. J For Sci 66:9–21

Barber CB, Dobkin DP, Huhdanpaa HT (1996) The Quickhull algorithm for convex hulls. ACM Trans Math Softw 22:469–483

Brazee NJ, Marra RE, Gocke L, Wassenaer PV (2011) Non-destructive assessment of internal decay in three hardwood species of northeastern North America using sonic and electrical impedance tomography. Forestry 84:33–39

Burcham DC, Brazee NJ, Marra RE, Kane B (2019) Can sonic tomography predict loss in load-bearing capacity for trees with internal defects? A comparison of sonic tomograms with destructive measurements. Trees Struct Funct 33:681–695. https://doi.org/10.1007/s00468-018-01808-z

Davis TAW, Richards PW (1934) The vegetation of Moraballi Creek, British Guiana: An ecological study of a limited area of tropical rain forest (Part II). J Ecol 22:106–155

Deflorio G, Fink S, Schwarze FWMR (2008) Detection of incipient decay in tree stems with sonic tomography after wounding and fungal inoculation. Wood Sci Technol 42:117–132

Divos F, Divos P (2005) Resolution of stress wave based acoustic tomography. Eberswalde, Germany, pp 309–314

Ennos AR (2012) Solid Biomechanics, 1st edn. Princeton University Press, Princeton, NJ, USA

Espinosa L, Brancheriau L, Cortes Y, et al (2020a) Ultrasound computed tomography on standing trees: Accounting for wood anisotropy permits a more accurate detection of defects. Ann For Sci 77:68

Espinosa L, Prieto F, Brancheriau L, Lasaygues P (2019) Effect of wood anisotropy in ultrasonic wave propagation: A ray-tracing approach. Ultrasonics 91:242–251

Espinosa L, Prieto F, Brancheriau L, Lasaygues P (2020b) Quantitative parametric imaging by ultrasound computed tomography of trees under anisotropic conditions: Numerical case study. Ultrasonics 102:106060

Gilbert EA, Smiley ET (2004) Picus sonic tomography for the quantification of decay in white oak (*Quercus alba*) and hickory (*Carya* spp.). J Arboric 30:277–281

Gilbert GS, Ballesteros JO, Barrios-Rodriguez CA, et al (2016) Use of sonic tomography to detect and quantify wood decay in living trees. Appl Plant Sci 4:1–13

Johnstone DM, Moore GM, Tausz M, Nicolas M (2010) The measurement of wood decay in landscape trees. Arboric Urban For 36:121–127

Kak A, Slaney M (2001) Principles of Computerized Tomographic Imaging. Society for Industrial and Applied Mathematics, Philadelphia, PA

Koeser AK, Hauer RJ, Klein RW, Miesbauer JW (2017) Assessment of likelihood of failure using limited visual, basic, and advanced assessment techniques. Urban For Urban Green 24:71–79

Kutner MH, Nachtsheim CJ, Neter J (2004) Applied Linear Regression Models, 4th edn. McGraw-Hill Irwin, Boston, MA, USA

Li L, Wang X, Wang L, Allison RB (2012) Acoustic tomography in relation to 2D ultrasonic velocity and hardness mappings. Wood Sci Technol 46:551–561

Liang S, Fu F (2012a) Strength loss and hazard assessment of Euphrates poplar using stress wave tomography. Wood Fiber Sci 44:1–9

Liang S, Fu F (2012b) Relationship analysis between tomograms and hardness maps in determining internal defects in Euphrates poplar. Wood Res 57:221–230

Liang S, Fu F (2014) Effect of sensor number and distribution on accuracy rate of wood defect detection with stress wave tomography. Wood Res 59:521–532

Liang S, Wang X, Wiedenbeck J, et al (2007) Evaluation of acoustic tomography for tree decay detection. In: 15th International Symposium on Nondestructive Testing of Wood. Duluth, MN, USA, pp 49–54

Liu L, Li G (2018) Acoustic tomography based on hybrid wave propagation model for tree decay detection. Comput Electron Agric 151:276–285

Marra RE, Brazee N, Fraver S (2018) Estimating carbon loss due to internal decay in living trees using tomography: implications for forest carbon budgets. Environ Res Lett 13:105004. https://doi.org/10.1088/1748-9326/aae2bf

Maurer H, Schubert SI, Bachle F, et al (2006) A simple anisotropy correction procedure for acoustic wood tomography. Holzforschung 60:567–573

Ostrovsky R, Kobza M, Gazo J (2017) Extensively damaged trees tested with acoustic tomography considering tree stability in urban greenery. Trees Struct Funct 31:1015–1023

Pearce RB (1996) Antimicrobial defences in the wood of living trees. New Phytol 132:203–233

Rabe C, Ferner D, Fink S, Schwarze FWMR (2004) Detection of decay in trees with stress waves and interpretation of acoustic tomograms. Arboric J 28:3–19

Rust S (2017) Accuracy and reproducibility of acoustic tomography significantly increase with precision of sensor position. J For Landsc Res 1:1–6

Rust S (2021) Comparison of methods to measure sensor positions for tomography. Arboric J. https://doi.org/10.1080/03071375.2020.1829374

Schubert S, Gsell D, Dual J, et al (2009) Acoustic wood tomography on trees and the challenge of wood heterogeneity. Holzforschung 63:107–112

Schwarze FWMR, Engels, J, Mattheck, C (2000) Fungal Strategies of Wood Decay in Trees. Springer-Verlag, Berlin, Germany

Schwarze FWMR, Lonsdale D, Mattheck C (1995) Detectability of wood decay caused by *Ustulina deusta* in comparison with other tree-decay fungi. Eur J For Pathol 25:327–341

Smiley ET, Matheny N, Lilly S (2017) Tree Risk Assessment, 2nd edn. International Society of Arboriculture, Champaign, IL, USA

Smith AP (1972) Buttressing of tropical trees: A descriptive model and new hypotheses. Am Nat 106:32–46

Wang LH, Xu HD, Zhou CL, Yang XC (2007a) Effect of sensor quantity on measurement accuracy of log inner defects by using stress wave. J For Res 18:221–225

Wang X, Allison RB, Wang L, Ross RJ (2007b) Acoustic tomography for decay detection in red oak trees. Forest Products Laboratory, Forest Service, US Department of Agriculture

Wang X, Wiedenbeck J, Liang S (2009) Acoustic tomography for decay detection in black cherry trees. Wood Fiber Sci 41:127–137

Table 1: Descriptive statistics of the number, size, and shape of cross sections measured using sonic tomography from temperate and tropical biomes

Biome	**Tomograms (*n*)**	**Cross-Sectional Area, *A* (m^2)**	**Circularity, *C* (dimensionless)**	**Solidity, *S* (dimensionless)**	**Eccentricity, *E* (dimensionless)**	**Percent Damaged Cross-Sectional Area, A_D (%)**
Temperate	51	0.18 (0.07, 0.33)	0.78 (0.59, 0.88)	0.98 (0.86, 0.99)	0.38 (0.07, 0.76)	34.0 (9.0, 58.0)
Tropical	21	1.13 (0.37, 2.23)	0.26 (0.07, 0.60)	0.69 (0.45, 0.95)	0.60 (0.31, 0.80)	33.3 (8.0, 63.9)

Note: The values listed in cells are mean (min, max). For more details about the individual cross sections measured with sonic tomography, see the original data used for analysis (https://doi.org/10.7910/DVN/RGJFMR).

Table 2: Analysis of variance of the effect of tree species on the accuracy of sonic tomograms A_D(error) (%)

Effect	df	F	p	Level	LS Mean (SE)
Species	3, 60	67.91	< 0.001	*A. saccharum*	-27.7 (3.1)a
				B. alleghaniensis	-23.2 (3.6)a
				F. grandifolia	-23.5 (2.8)a
				P. indicus	32.0 (3.2)b

Note: LS means followed by the same letter are not significantly different at the $\alpha = 0.05$ level.

Table 3: Parameter estimates, confidence intervals, and coefficients of determination for linear regression models describing the relationship between the accuracy of sonic tomograms, A_D(error) (%), and four geometric properties of the measured cross sections

	Cross-Sectional Area, *A* (m^2)	**Circularity, *C* (dimensionless)**	**Solidity, *S* (dimensionless)**	**Eccentricity, *E* (dimensionless)**
VB				
Intercept	-29.8	49.9	132.0	-49.6
(95% CI)	(-35.4, 24.1)	(41.2, 58.7)	(111.0, 152.9)	(-66.0, 33.1)
Slope	44.2	-94.4	-157.8	89.1
(95% CI)	(35.6, 52.8)	(-107.1, 81.7)	(-180.7, 134.8)	(54.3, 123.9)
r^2	0.60	0.76	0.73	0.27
GVB				
Intercept	-19.5	68.4	160.7	-42.9
(95% CI)	(-25.3, 13.6)	(59.8, 77.1)	(140.5, 181.0)	(-60.2, 25.7)
Slope	48.8	-104.0	-176.0	102.0
(95% CI)	(39.9, 57.7)	(-116.7, 91.4)	(-198.2, 153.9)	(65.4, 138.5)
r^2	0.63	0.79	0.78	0.31

Note: Using the default settings (SoT 1 – default) for the PiCUS® Q74 software, the models were fit to observations (n = 72) computed by selecting damaged areas in tomograms with violet and blue (VB) or green, violet, and blue (GVB), respectively. See the methods section for more information about the four geometric properties depicting the size and shape of cross sections.

Table 4: Analysis of covariance of the effects of software settings and color interpretation on the accuracy of sonic tomograms, A_D(error) (%)

Effect	**df**	***F***	***p***	**Level**	**Parameter estimate (95% CI)**	***p***
Settings	3, 563	25.65	< 0.001	SoT 1 – Default	-3.9 (-5.8, 1.9)	< 0.001
				SoT 1 – Expanded	-9.3 (-11.2, 7.3)	< 0.001
				SoT 2 – Default	-12.0 (-14.0, 10.1)	< 0.001
				SoT 2 - Expanded	-15.8 (-17.7, 13.9)	< 0.001
Colors	1, 563	140.75	< 0.001	VB	-16.1 (-17.5, 14.7)	< 0.001
				GVB	-4.4 (-5.8, 3.0)	< 0.001
Settings × Colors	3, 563	1.85	0.1375			
G × Settings	3, 563	32.36	< 0.001	SoT 1 – Default	-26.0 (-28.0, 24.1)	< 0.001
				SoT 1 – Expanded	-17.3 (-19.3, 15.4)	< 0.001
				SoT 2 – Default	-18.6 (-20.6, 16.7)	< 0.001
				SoT 2 - Expanded	-12.3 (-14.3, 10.3)	< 0.001
G × Colors	1, 563	18.49	< 0.001	VB	-16.4 (-17.8, 15.0)	< 0.001
				GVB	-20.7 (-22.1, 19.3)	< 0.001

Note: The fixed effects included in the model were the settings used to produce sonic tomograms with the PiCUS® Q74 software: SoT 1 calculation with the default maximal color space (SoT 1 – default), SoT 1 calculation with the expanded maximal color space (SoT 1 – expanded), SoT 2 calculation with the default maximal color space (SoT 2 – default), and SoT 2 calculation with the expanded maximal color space (SoT 2 – expanded); the colors used to interpret the extent of damaged wood in tomograms: violet and blue (VB) and green, violet, and blue (GVB), and their interaction: settings × colors. The geometry covariate, G (dimensionless), used for the model depicted covariation in the cross-sectional area, A (m^2), circularity, C (dimensionless), and solidity, S (dimensionless), of measured tree parts along a single axis determined using Principal Components Analysis, and the fixed effects were tested at the mean value of the covariate ($G = 0$). Computed from the factorial model, the parameter estimates depict the intercept (conditional effects) and slope (marginal effects) coefficients for the fixed effects and covariates, respectively.

Table 5: Mean separation for the analysis of covariance of the effects of software settings and color interpretation on the accuracy of sonic tomograms, A_D(error) (%)

Geometry	-2.77	0	0.85
Settings			
SoT 1 – default	68.2 (2.9)a	-3.9 (1.0)a	-26.0 (1.3)ab
SoT 1 – expanded	38.7 (2.9)b	-9.3 (1.0)b	-24.0 (1.3)b
SoT 2 – default	39.5 (2.9)b	-12.0 (1.0)c	-27.8 (1.3)a
SoT 2 – expanded	18.3 (2.9)c	-15.8 (1.0)d	-26.3 (1.3)ab
Colors			
VB	29.4 (2.1)a	-16.1 (0.7)a	-30.1 (0.9)a
GVB	53.0 (2.1)b	-4.4 (0.7)b	-22.0 (0.9)b

Note: The values listed in cells are least-squares (LS) means (SE). For each fixed effect at three values of the geometry covariate, LS means followed by the same letter are not significantly different at the α = 0.05 level.

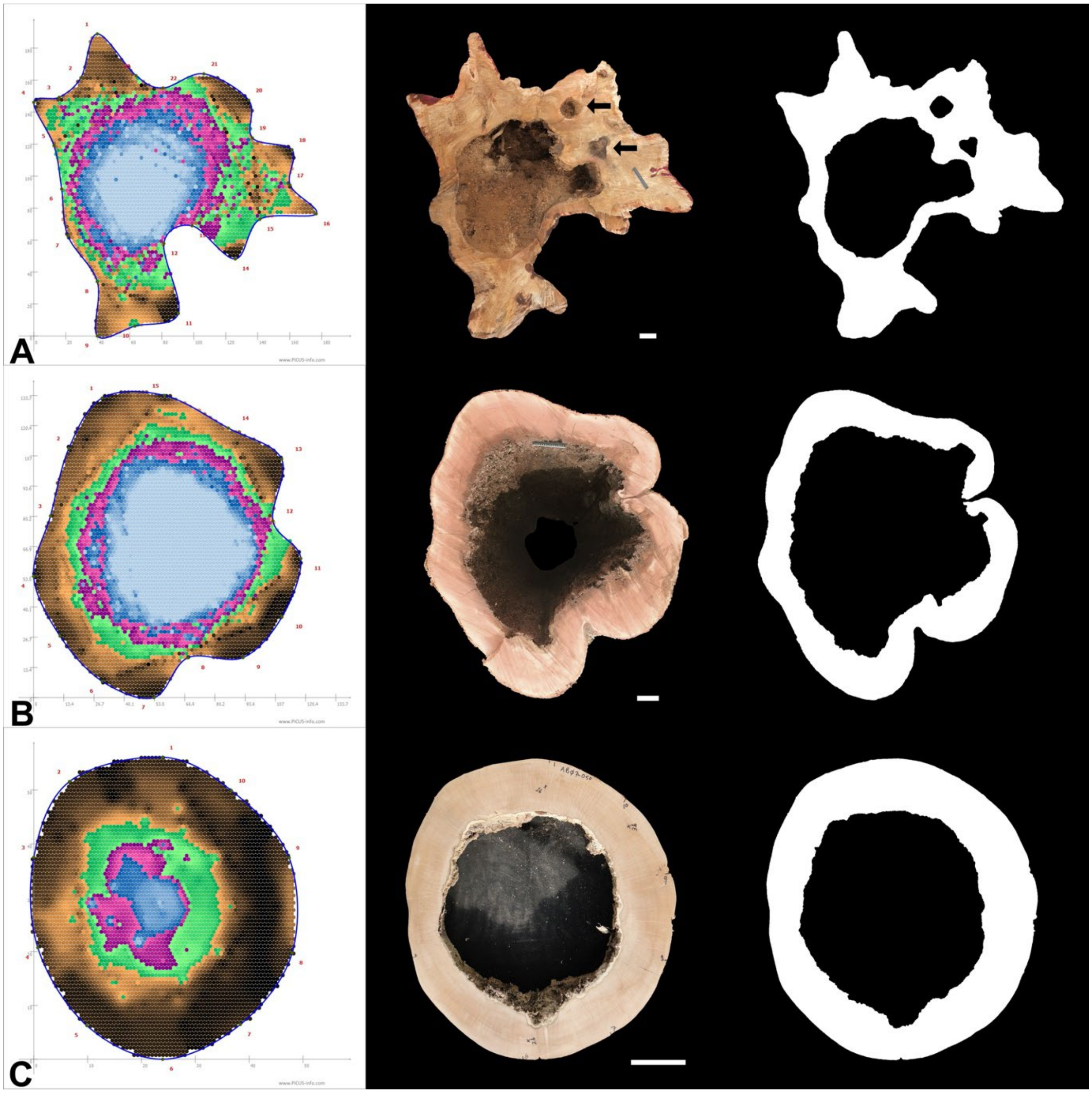

Figure 1: Using the PiCUS Sonic Tomograph 3, the accuracy of sonic tomography was examined by comparing tomograms (left) with the destructively measured internal condition (center) of trees with different cross-sectional geometries, including large, irregularly-shaped (**A**), large, round (**B**), and small, circular trees (**C**). For reference, the length of the white scale bar is 10 cm, and the default calculation method (SoT 1) was used to create the displayed tomograms. The reference photographs were manually converted into binary images (right), in which black (0) and white (1) represented the absence or presence, respectively, of solid wood. The extent of damaged wood depicted by specific colors in each tomogram was compared with the corresponding binary image. Using the default software settings, the amount of damage depicted in tomograms was noticeably greater (**A**) and less (**C**) than the actual extent of damaged wood in the large, concave (A = 1.58 m^2, S = 0.72) angsana (*Pterocarpus indicus*) and small, circular (A = 0.16 m^2, S = 0.99) American beech (*Fagus grandifolia*), respectively. In contrast, the amount of damage was more reasonably depicted (**B**) in the large, convex santol (*Sandoricum koetjape*) section (A = 1.18 m^2, S = 0.95). Some tropical trees contained longitudinal voids (black arrows) formed by the natural grafting of adjacent buttress roots, and the voids were classified as damaged wood for comparison with tomograms, since they would similarly impede acoustic wave transmission.

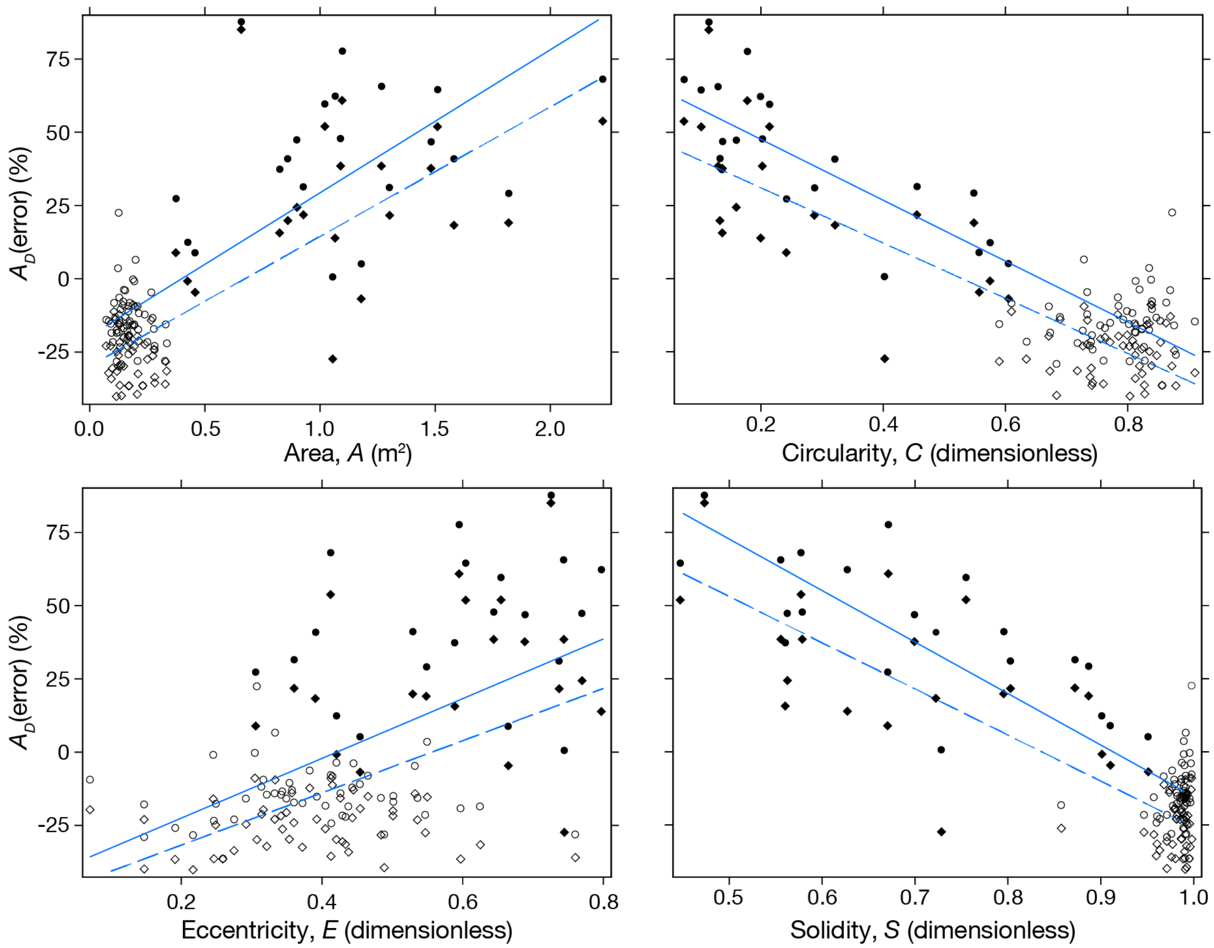

Figure 2: Scatter plots and least squares regression lines of the actual difference between the percent damaged cross-sectional area determined using sonic tomography and destructive measurements, A_D(error) (%), against four different geometric properties of the measured temperate (open symbols) and tropical (filled symbols) cross sections, including, clockwise from upper left, cross-sectional area, A (m^2); circularity, C (dimensionless); solidity, S (dimensionless); and eccentricity, E (dimensionless). Using the default calculation settings (SoT 1 – default) for the PiCUS® Q74 software, the dashed and solid lines depict linear models fit to observations computed by selecting damaged areas in tomograms with violet and blue (diamonds) or green, violet, and blue (circles), respectively. See Table 3 for model parameter estimates and fit statistics.